Direct Nuclear-Pumped Lasers Using the $^3He(n,p)^3H$ Reaction

R. J. DeYoung*
Miami University, Oxford, Ohio
and
N. W. Jalufka† and F. Hohl‡
NASA Langley Research Center, Hampton, Va.

Direct nuclear pumping of gas lasers has been achieved using the $^3He(n,p)^3H$ nuclear reaction. Nuclear lasing was demonstrated in ^3He-Ar (1.27, 1.79 μm), ^3He-Xe (2.026 μm), ^3He-Kr (2.19, 2.52 μm) and ^3He-Cl (1.587 μm). Total pressures ranged from 300 Torr to 4 atm with thermal neutron fluxes of from 10^{15}-10^{17} neutrons/cm^2-s. A peak power of 3.7 W was obtained from ^3He-Ar (1.79 μm) at a total pressure of 4 atm with a thermal flux of 1.0×10^{17} neutrons/cm^2-s. The lowest thermal flux lasing threshold was found for the ^3He-Xe (4×10^{15} neutrons/cm^2-s) system. Population inversion mechanisms are discussed and it is shown that collisional radiative recombination of the atomic minority species ion is thought to be the dominant pumping mechanism.

Introduction

RESEARCH on direct nuclear-pumped lasers has progressed rapidly since this new form of laser excitation became a reality in 1975. Recently, these lasers have received increasing attention as their output power has increased (from milliwatts to watts) and as the thermal neutron flux lasing threshold has been reduced (from 10^{16} to 10^{14} neutrons/cm^2-s). With such rapid progress, direct nuclear-pumped laser research is beginning to emerge from the infant stage. The full potential of these lasers is presently not known, but certain important characteristics are apparent[1]: 1) potential for high steady-state laser power output; 2) a well designed reactor laser should be physically very compact and lightweight; and 3) the potential for high laser efficiency at high gas pressures.

Potential applications of direct nuclear-pumped lasers are numerous, especially where high power lasers are required in remote locations. For example, a nuclear laser system could be placed in Earth orbit, supplying power to satellites, space stations, and lunar bases, which would no longer require individual power generation systems. The high-power laser output could also be used for propulsion, such as moving large space structures to synchronous orbit from low Earth orbit. The laser radiation would be absorbed on a solid or liquid propellant surface, causing rapid evaporation of the surface.[2] The high-temperature gaseous plasma would then rapidly expand, producing a very high specific impulse.

Terrestrial applications would include steady-state laser fusion and isotope separation. Here, the important advantage is the inherent high-power steady-state operation of the nuclear laser system.

In this paper, we present experimental results on a specific class of direct nuclear-pumped lasers classified as "volumetric nuclear lasers." Earlier nuclear lasers used either a uranium-235 or boron-10 coating on the internal surface of the laser cell to excite CO (Ref. 3), He-Xe (Ref. 4), Ne-N_2 (Ref. 5), and He-Hg (Ref. 6). The fission fragments or α-particles ionized the background gas, creating secondary electrons which in turn excited the lasing medium. The major disadvantage with coating excitation is that more than 50% of the nuclear reaction energy is lost by the particles traversing the coating material. Coatings are therefore inherently inefficient. At high pressure fission fragments do not penetrate deeply into the lasing media and, thus, excitation occurs only in a thin region near the coating surface.

A more efficient system is obtained if a fissioning gas ix mixed with the lasing gas to form a homogeneous mixture, resulting in uniform volume excitation. A logical fissioning gas is He-3 because of its large thermal neutron cross section for the $^3He(n,p)^3H$ reaction (5300b). In previous work,[7] gain was observed in a ^3He-Ne-O_2 plasma at 8446 Å OI when the mixture was subjected to a thermal neutron pulse of 2.5×10^{15} neutrons/cm^2-s. Lasing was not achieved in this mixture, but the potential for pumping gas lasers by the ^3He reaction was demonstrated. Lasing in ^3He-Ar (Refs. 8 and 9) and ^3He-Xe (Refs. 10 and 11), was subsequently achieved using a fast-burst reactor.

Reactor Experimental Setup

The cross section of a typical volumetric nuclear laser is illustrated in Fig. 1. A fast-burst reactor is used as a source of

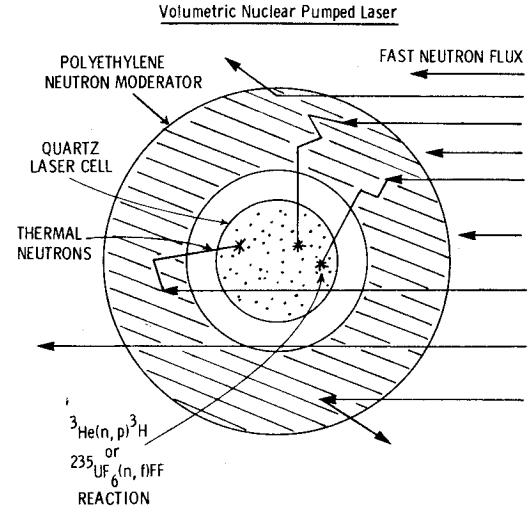

Fig. 1 Schematic representation of a volumetric direct nuclear-pumped laser. The quartz laser cell containing ^3He plus a lasing gas is surrounded by a polyethylene moderator which thermalizes neutrons created by a fast-burst reactor. The laser medium is then excited by the $^3He(n,p)^3H$ reaction.

Presented as Paper 78-66 at the AIAA 16th Aerospace Sciences Meeting, Huntsville, Ala., Jan. 16-18, 1978; submitted Feb. 23, 1978; revision received June 9, 1978.

Index category: Lasers.

*Assistant Professor.
†Research Scientist.
‡Head, Space Technology Branch. Member AIAA.

neutrons which penetrate a polyethylene moderator. Here the fast neutrons are thermalized to take advantage of the large (5300b) $^3He(n,p)^3H$ thermal cross section. After thermalization, neutrons scatter into the laser cell, which contains a mixture of He-3 and some lasing gas. Nuclear reactions then occur which produce a proton of 0.56 MeV and a tritium ion of 0.19 MeV, and these ions in turn produce secondary electrons which then pump the laser medium creating a population inversion.

Figure 2 shows a typical reactor experimental setup. The polyethylene moderator used in the experiments reported here is 60-cm long with an annular thickness of 5 cm. The laser cell consists of 2.5-cm o.d. quartz tubing (80-cm long) with Brewster angle quartz windows at each end. A variety of 2.5-cm-diameter dielectric coated mirrors (typical reflectivity $\approx 98.5\%$) were used to form optical cavities approximately 100 cm in length. A high vacuum and gas-handling system is attached to the laser cell which achieves vacuums on the order of 10^{-6} Torr. All gases are allowed to mix in the laser cell for approximately 45 min before nuclear excitation.

Electrodes are attached to the laser cell which enable a low-pressure gas mixture to be pulsed electrically. With electric excitation, the cavity mirrors and detectors can be aligned. Apertures are inserted into the optical cavity in front of each laser mirror to allow lasing only along the centerline of the optical cavity.

The fast-burst reactor used in the experiments reported here is the U.S. Army Pulse Radiation Facility reactor at Aberdeen, Md. This reactor has a capability of 1.5×10^{17} neutrons/cm^2-s inside this specific polyethylene geometry. The fast neutron pulse halfwidth is 50 μs but, after thermalization, the moderated neutron pulse halfwidth is lengthened to about 200 μs. The reactor core is 20-cm high with a 22-cm diameter. Normally, five high-yield pulses ($\sim10^{17}$ neutrons/cm^2-s) can be achieved per day; for low-yield pulses (n $\sim10^{15}$ neutrons/cm^2-s) this can be increased to about 10 per day.

The laser detection optics are located 15 m from the laser cavity and consist of an iris and lens to focus the light onto an InAs detector. A variable filter wheel (100 Å full width half maximum) can be used to select only one lasing transition of interest.

The InAs detector (wavelength response is from 1.2 to 3.8μ) was used to monitor all laser emission. This detector was found to have a very low sensitivity to γ-ray and neutron irradiation and thus no shielding was required. Signals from the InAs detector were sent directly to an oscilloscope with 1000 Ω termination.

The thermal neutron pulse is measured by a cobalt self-powered flux detector, the signal being sent to an oscilloscope with 1000 Ω termination. This detector is 60-cm long and is placed inside the 60-cm long polyethylene moderator next to the quartz tube. The detected signal is the average thermal neutron flux along the 60-cm moderator. The detector was found to be insensitive to γ-ray and fast-neutron irradiation.

Light in the visible spectrum is transmitted through the back laser mirror and is then focused onto the slits of a ⅓-m monochromator which disperses the light and focuses it onto a vidicon optical multichannel analyzer. The optical multichannel analyzer output is fed into a programable calculator where the spectral data are stored on tape as well as plotted. Data on lasing and spectral emission can be gathered simultaneously during each reactor pulse.

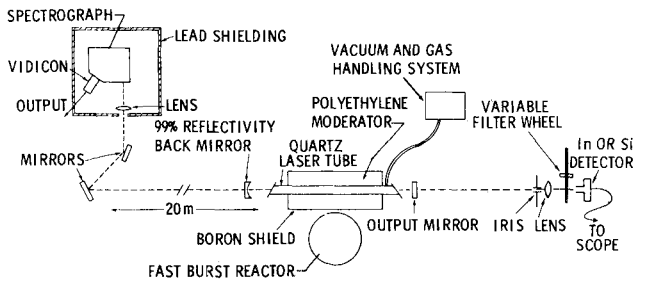

Fig. 2 Typical reactor experimental setup indicating the location of lasing detection optics and optics for detection of the visible spectrum emitted from the laser cell.

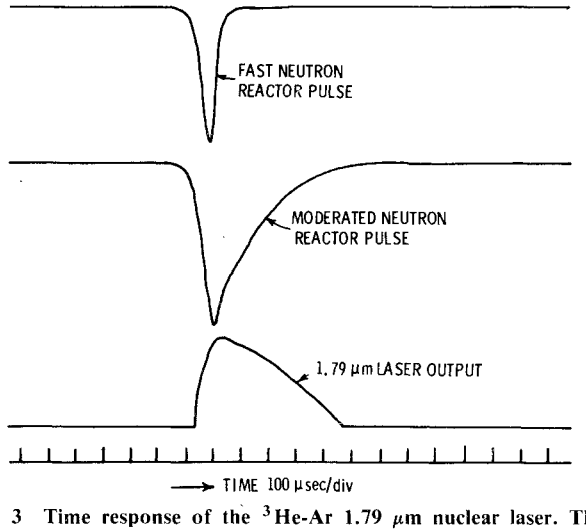

Fig. 3 Time response of the ^{3}He-Ar 1.79 μm nuclear laser. The neutron pulse generated by the fast-burst reactor is moderated by the polyethylene geometry and thus is lengthened in time. The ^{3}He-Ar laser output follows the time response of the moderated neutron pulse.

^{3}He-Ar Direct Nuclear Pumping Results

The ^{3}He-Ar (Refs. 8 and 9) (1.79μm ArI, $3d\ [1/2]^0_1 - 4p[3/2]_2$ or $3d[1/2]^0_0 - 4p[3/2]_1$), (1.27μm ArI, $3d'[3/2]^0_1 - 4p'[1/2]_1$), system was the first volumetric direct nuclear-pumped laser and demonstrated that the $^3He(n,p)^3H$ reaction could deposit sufficient energy into the gas medium for lasing. Figure 3 shows a typical recording of the laser output. Fast neutrons from the fast-burst reactor are moderated by the polyethylene which broadens the pulse shape to that shown in the figure. The thermal neutrons produce $^3He(n,p)^3H$ reactions within the laser cell which, in turn, ionize and excite the He-Ar gas mixture inducing lasing, as shown in the lower trace of Fig. 3. Lasing is initiated with a sharp lasing threshold, a characteristic of all gas lasers, and laser output continued to follow the thermal neutron pulse as opposed to the fast neutron pulse, demonstrating that the thermal neutrons actually pump the laser system. Since lasing lasted much longer than the upper laser level lifetime, the He-Ar laser can be considered a steady-state system.

In Fig. 4, the 1.79 μm ArI laser output is shown as a function of ^{3}He-Ar pressure for a fixed 1% Ar concentration and 1×10^{17} neutron/cm^2-s thermal neutron flux pulses. The laser cavity consisted of two dielectric mirrors, each with 1% transmission at 1.7 μm. Laser output continues to increase with total pressure until approximately 2 atm, above which lasing output tends to saturate even though increasing power is deposited in the gas. The cause of this saturation is not completely understood, but is thought to be due to plasma effects such as pressure broadening of the laser line and collisional depopulation of the upper laser level. The solid curve shows the calculated power deposition in the laser cavity mode volume. At 2 atm the peak laser output was 3.4 W and the power deposited in the mode volume was 3.8 kW, thus the efficiency is 0.09%. If the power deposited in the total laser tube volume is used, the efficiency would be 1×10^{-3}%.

An argon concentration study was carried out to determine the optimum lasing concentration. These results, as shown in Fig. 5, indicate that the optimum argon concentration for peak lasing output is near 1.0%.

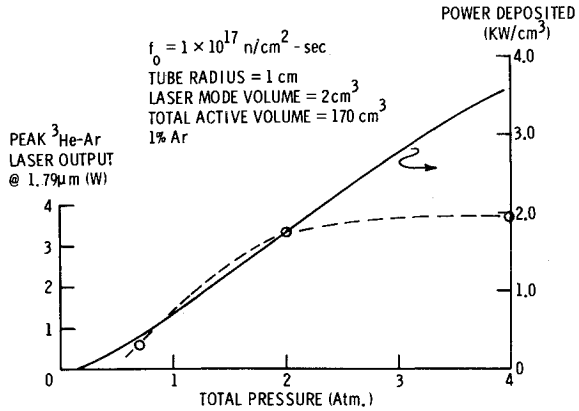

Fig. 4 Calculated power deposition in a laser tube of 1-cm radius normalized at 2 atm (—) with the experimental nuclear lasing results (○). Above 2 atm power deposition continues to increase, whereas lasing output saturates.

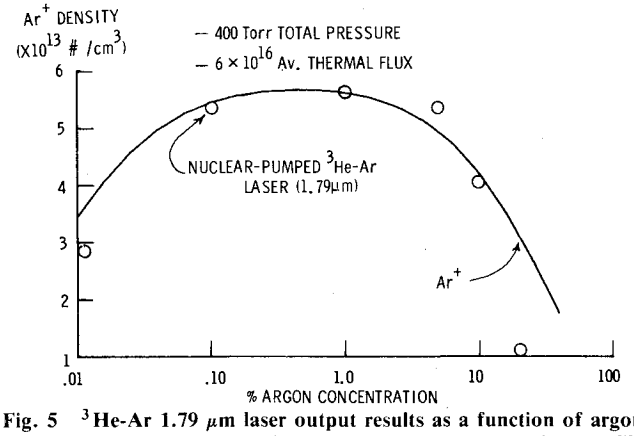

Fig. 5 ^{3}He-Ar 1.79 μm laser output results as a function of argon concentration. Also shown is the calculated concentration profile determined from Eq. (1) and normalized to the experimental data at 1% Ar.

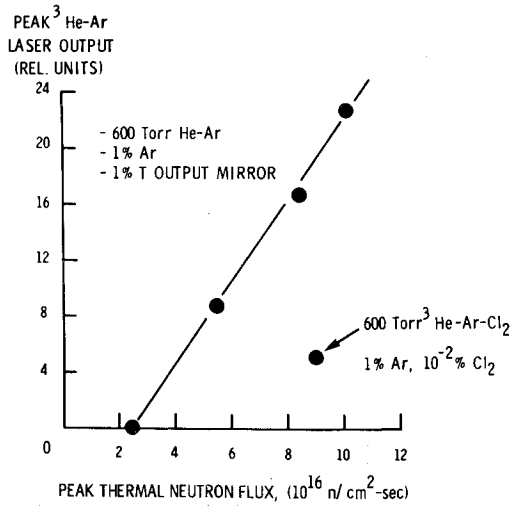

Fig. 6 He-Ar 1.79 μm laser output as a function of peak thermal neutron flux. A sharp lasing threshold was found at 2.5×10^{16} neutrons/cm^2-s.

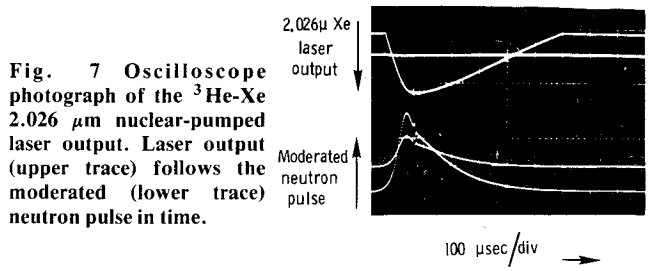

Fig. 7 Oscilloscope photograph of the ^{3}He-Xe 2.026 μm nuclear-pumped laser output. Laser output (upper trace) follows the moderated (lower trace) neutron pulse in time.

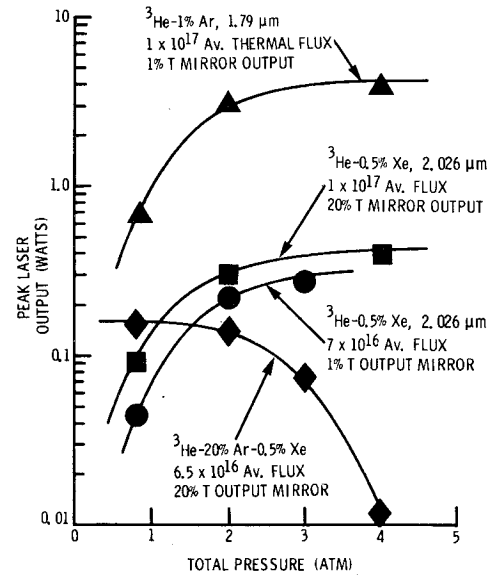

Fig. 8 Peak nuclear laser output vs total pressure in atmospheres for the ^{3}He-Ar and ^{3}He-Xe systems. Nearly 4 W was achieved with the ^{3}He-Ar 1.79 μm laser at 4 atm. Peak lasing at 2.026 μm in ^{3}He-Xe was 0.35 W using a 20% transmission output mirror. Addition of 20% Ar to ^{3}He-Xe resulted in increased output at 600 Torr, but lasing decreased at higher pressures.

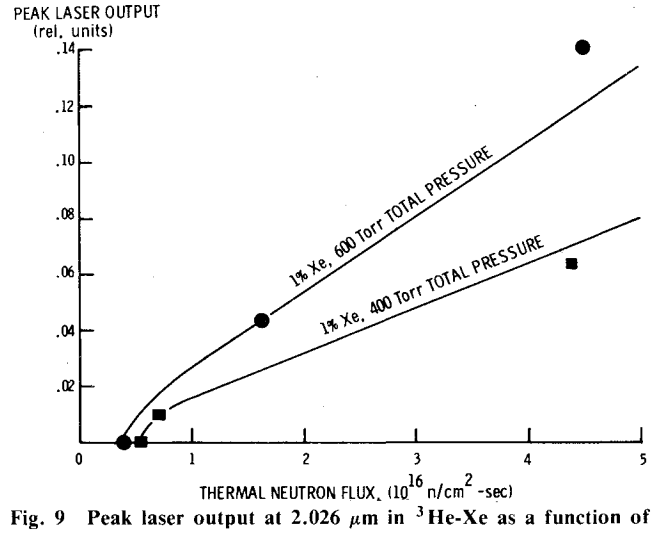

Fig. 9 Peak laser output at 2.026 μm in ^{3}He-Xe as a function of thermal neutron flux. The thermal neutron lasing threshold flux was 0.4×10^{16} neutrons/cm^2-s. With higher fluxes, lasing was directly proportional to thermal flux as shown by the proximity of the data points to the line drawn proportional to flux.

The scaling of laser output with thermal neutron flux is shown in Fig. 6. Here the total pressure of ^{3}He-Ar was held constant at 600 Torr (1% Ar). Lasing threshold occurred at a thermal neutron flux of 2.5×10^{16} neutrons/cm^2-s, and laser output continued to rise linearly with increasing neutron flux. At fluxes higher than those shown in Fig. 6, the laser output is expected to be directly proportional to thermal neutron flux as in the ^{3}He-Xe nuclear laser.

A small amount of Cl_2 (10^{-2}%) was added to ^{3}He-Ar at 600 Torr to depopulate the lower laser level. Lasing output did not improve but actually decreased, as shown in Fig. 6.

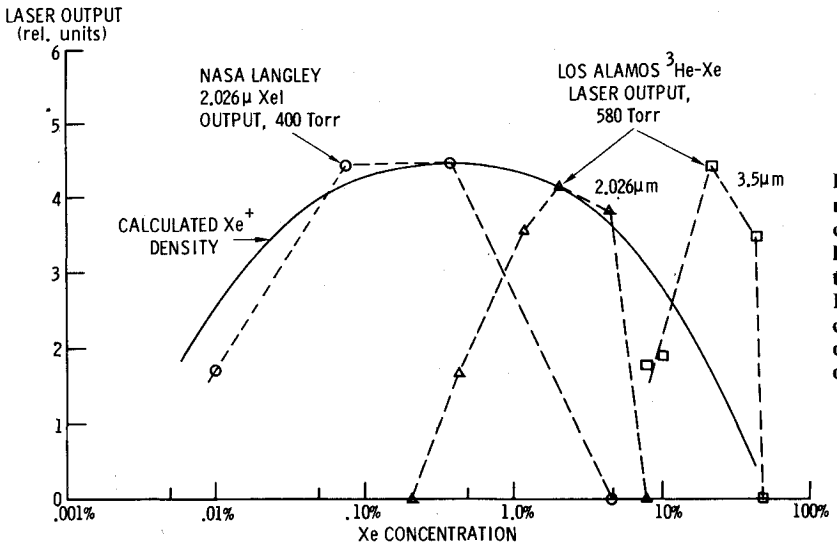

Fig. 10 ^{3}He-Xe laser concentration profile after normalization. The data obtained for this paper (○) are compared to the results of Los Alamos (Δ) for 2.026 μm lasing. The calculated Xe^+ density has been normalized to the experimental data. Also plotted are the results of Los Alamos (□) on ^{3}He-Xe lasing at 3.5 μm. The concentration profile of the 3.5 μm lasing is dramatically different from lasing at 2.026 μm, thus different excitation processes appear to be involved.

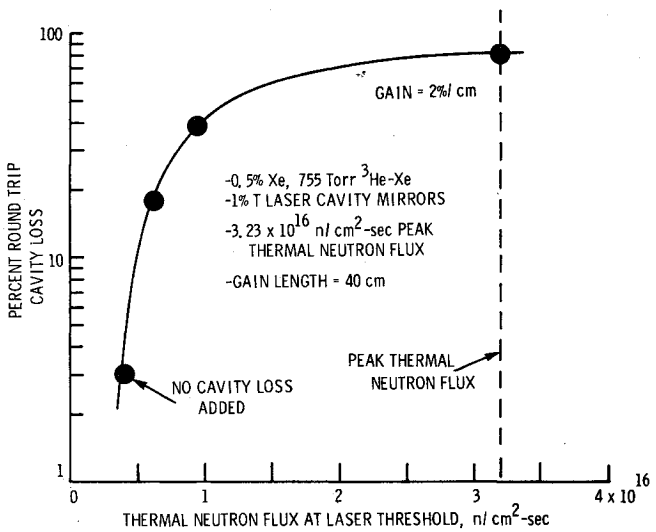

Fig. 11 The gain of the ^{3}He-Xe 2.026 μm system was measured by adding stepwise increasing amounts of attenuation in the laser cavity. As the added attenuation was increased, the thermal neutron lasing threshold also increased up to 3.1×10^{16} neutrons/cm^3-s where the lasing threshold equalled the peak of the neutron pulse, and thus no lasing occurred. The gain was found to be approximately 2.0%/cm.

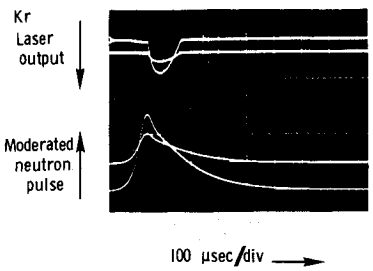

Fig. 12 Oscilloscope photograph of the ^{3}He-Kr 2.5 μm nuclear-pumped output. Lasing threshold takes place near the peak of the moderated neutron pulse.

^{3}He-Xe Direct Nuclear Pumping Results

Figure 7 is a typical oscilloscope photograph of the ^{3}He-Xe (2.026μm XeI, $5d[3/2]_1^0 - 6p[3/2]_1$) direct nuclear-pumped laser. As with ^{3}He-Ar, the laser output exhibits a sharp threshold and lasing follows the moderated neutron pulse. The neutron flux lasing threshold was found to be 4×10^{15} neutrons/cm^2-s which is the lowest threshold for any He-3 direct nuclear-pumped laser to date. Lasing FWHM is approximately 400 μs, thus it can be considered to be a quasi-steady-state system since the atomic and molecular processes in the gas occur on a much shorter time scale.

In Fig. 8, the ^{3}He-Xe laser output is shown as a function of total pressure. As was the case for ^{3}He-Ar, laser output tends to saturate with increasing pressure above 2 atm. In an attempt to increase the laser output power, the 1% transmission output mirror was replaced with a mirror of 20% transmission at 2 μm. Laser output increased only slightly, as shown in Fig. 8. The output of the He-Xe laser can also be increased by adding Ar (Ref. 12). During the discharge the dimer Ar_2^* forms very rapidly and the close resonance between Ar_2^* and the upper laser level of XeI (2.026 μm laser) allows additional pumping of the Xe $5d\,(3/2)_1^0$ upper laser level, thus enhancing laser output. This was found to occur in the nuclear generated plasma, but only at lower pressures (~600 Torr ^{3}He-Xe-Ar). As the total pressure increased, XeI (2.026 μm) lasing decreased for a fixed concentration of 20% Ar.

The variation of 2.026 μm laser output with peak thermal neutron flux is shown in Fig. 9. Both sets of data were taken at 1% Xe concentration, but with slightly different total pressures (400 and 600 Torr ^{3}He-Xe). It was found that peak laser output was directly proportional to thermal flux over the flux range investigated, as shown by the proximity of the data points to the solid lines. The thermal neutron flux lasing threshold was approximately 0.4×10^{16} neutrons/cm^2-s.

A concentration study of XeI (2.026 μm) lasing was undertaken, with the results shown in Fig. 10. Optimum Xe concentration was found to be near 0.1% Xe. Also plotted, after normalization to our data, are results obtained at the Los Alamos Scientific Laboratory[11] showing their concentration study for both the 2.026 μm and the 3.5 μm (XeI) lasing transitions. The Los Alamos results for the optimum concentration of Xe differ by an order of magnitude which is not completely understood at present.

The gain of the ^{3}He-Xe (2.026 μm) laser was measured for a constant 0.5% Xe concentration, 755 Torr ^{3}He-Xe pressure, and 3.23×10^{16} neutrons/cm^2-s peak thermal flux pulses. The results are shown in Fig. 11 where the percentage of round trip cavity loss is plotted as a function of the laser threshold thermal neutron flux. Calibrated (at 2 μm) neutral density filters were mounted on the Brewster angle window to stepwise increase the loss in the laser cavity. With no added filter loss, the cavity losses from the Brewster windows and laser mirror transmission were ~3%. Adding neutral density filters increased the laser threshold neutron flux until a loss of 80% was reached. At that point, the laser threshold neutron flux must be very near the peak of the neutron pulse (no lasing occurred) and thus the round-trip cavity losses must equal the round-trip gain. The gain was approximately 2.0% cm^{-1},

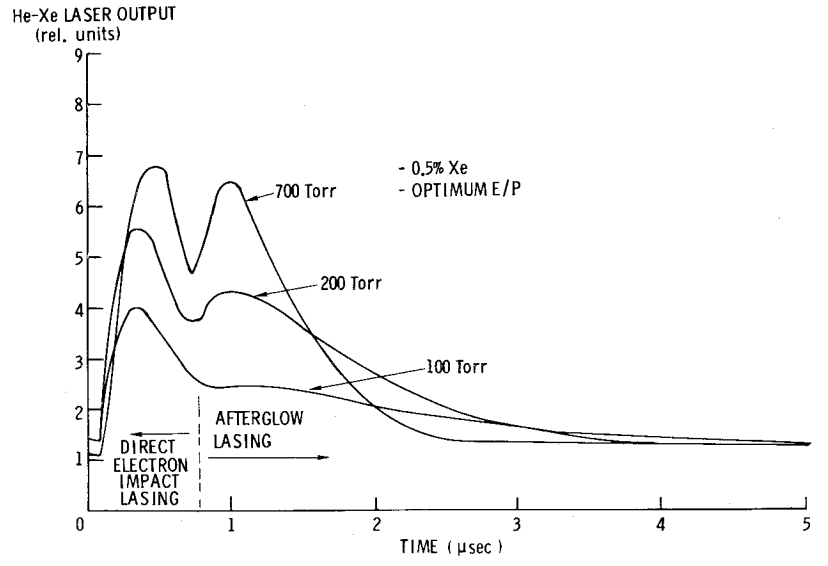

Fig. 13 Typical results for He-Xe 2.026 μm electrically pulsed lasing (TEA discharge). There are two distinct lasing regions. The first region, which follows the current pulse, is lasing by direct electron impact excitation followed by the second, or afterglow, lasing region. The afterglow region was found to characterize the nuclear-induced plasma.

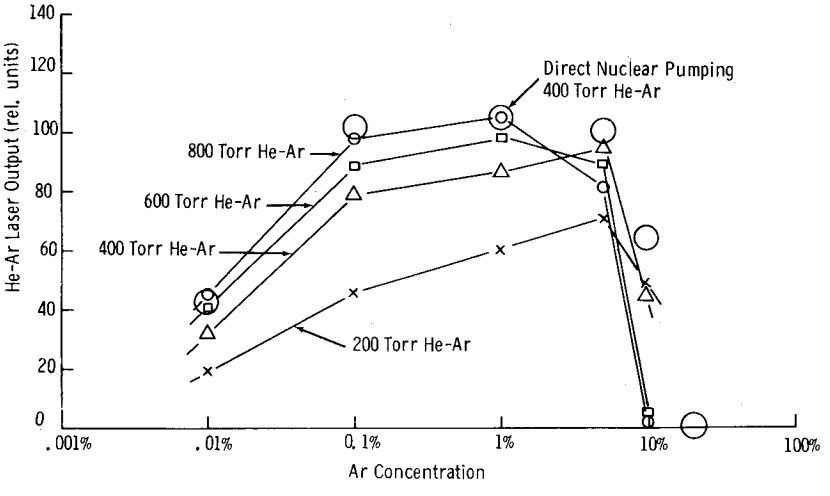

Fig. 14 Results of electrically pulsed afterglow lasing in He-Ar 1.79 μm compared with nuclear-pumped lasing of ^{3}He-Ar (400 Torr ^{3}He-Ar) after normalization at 1% Ar concentration. There is a close agreement, at high pressures, between the afterglow and nuclear-pumped laser data as a function of Ar concentration.

which is a reasonably high gain and, in part, explains why it has such a low thermal neutron flux lasing threshold.

^{3}He-Kr Direct Nuclear Pumping Results

Shown in Fig. 12 is the ^{3}He-Kr direct nuclear-pumped laser output at 0.5% Kr concentration, 400 Torr ^{3}He-Kr, and a peak thermal flux of 1.55×10^{17} neutrons/cm^2-s. The filter wheel was used to determine lasing at both 2.52 μm and 2.19 μm. Considerably reduced laser output was found at the 2.19 μm KrI, $4d[3/2]_2^0 - 5p[3/2]_2$, transition, thus is it assumed that most of the He^3-Kr laser output is due to the 2.52 μm $4d[1/2]_1^0 - 5p[3/2]_2$ transition. Under electrical excitation, the above lines were the only two lasing transitions that lased in the afterglow using the same optical cavity. The cavity consisted of two 2-m radius of curvature mirrors, each with 95% reflectivity at 2.5 μm. The mirror separation was 80 cm. The Kr concentration (0.5%) should have been near optimum as determined from electrical afterglow measurements. The high laser threshold thermal neutron flux is probably the result of both laser transitions (2.19 μm and 2.52 μm) feeding into the same lower laser level, thus quenching further lasing or alternately increasing the lasing threshold. Both transitions can lase simultaneously due to the broad high reflectivity bandwidth of the 2.5 μm dielectric mirrors.

^{3}He-Cl Direct Nuclear Pumping Results

A mixture of ^{3}He-Cl (0.008% Cl, 600 Torr total pressure) was found to lase at 1.587 μm (Refs. 13 and 14) ($3d^4F_{9/2} - 4p^4D_{7/2}$) with similar time characteristics as the ^{3}He-Ar and ^{3}He-Xe lasers. The laser cavity consisted of two 2-m radius of curvature mirrors coated for peak reflectivity at 1.7 μm (1.6% transmission at 1.59 μm). The thermal neutron flux threshold was approximately 7×10^{15} neutrons/cm^2-s and the laser output power was near 0.1 W peak. When the concentration of Cl was increased to 0.17% Cl, no lasing was observed, thus the CL laser operates at significantly lower concentrations than the Ar, Xe, or Kr lasers.

Simulation of Direct Nuclear-Pumped Lasers by the High-Pressure Electrically Pulsed Afterglow Laser

Through research on high-pressure (>50 Torr) electrically pulsed lasers, it was found that lasing in He-Xe, for example, occurred in two distinct regions. Figure 13 shows typical results of electrically pulsed (transverse excited atmospheric discharge) lasing at 2.026 μm in He-Xe. The first lasing region corresponds to direct electron impact excitation of the upper laser level (or levels slightly above) since lasing follows the current pulse. The second region represents afterglow lasing where there are no external excitation sources and the plasma is simply decaying in time. In this region recombination is the dominant plasma loss mechanism, since diffusion is negligible at these higher pressures. A direct nuclear-pumped plasma consists primarily of near-thermal electrons, likewise the afterglow region of an electrically pulsed discharge consists of near-thermal electrons since there are no electric fields to heat the thermalizing electrons. Thus, the afterglow electrical laser should be a good simulation of a nuclear induced laser.

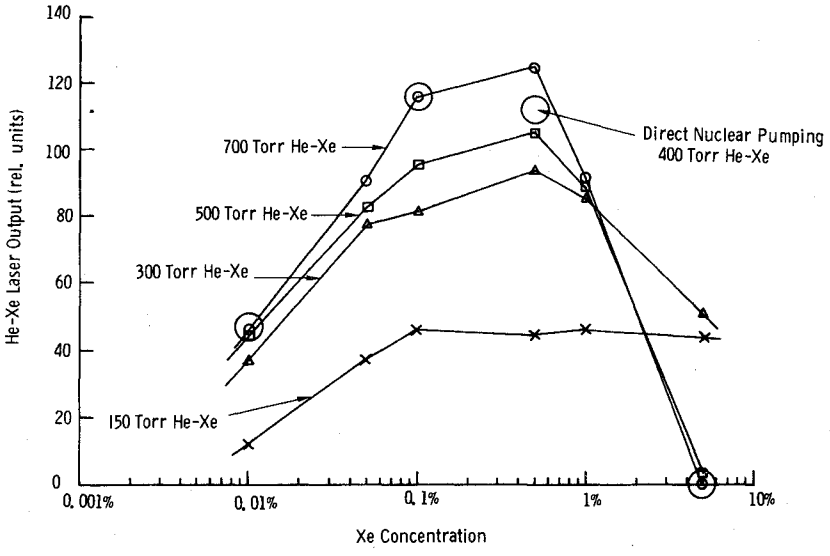

Fig. 15 Results of electrically pulsed afterglow lasing on He-Xe 2.026 μm compared with nuclear-pumped lasing (400 Torr ^{3}He-Xe) after normalization at 0.1% Xe concentration. At high pressures there is a close correlation between afterglow and nuclear-pumped lasing as a function of Xe concentration.

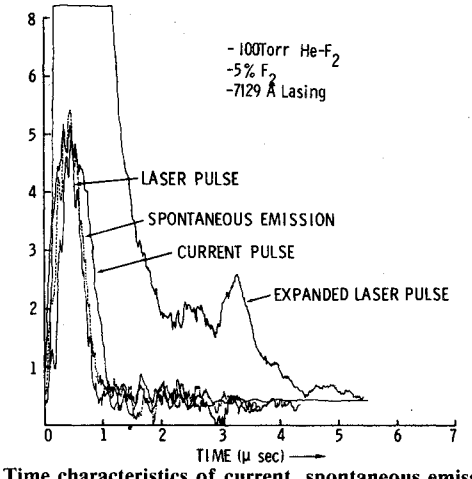

Fig. 16 Time characteristics of current, spontaneous emission, and lasing at 7129Å in He-F_2 (100 Torr). There is a close correlation between the lasing pulse and the current pulse with little lasing in the afterglow region.

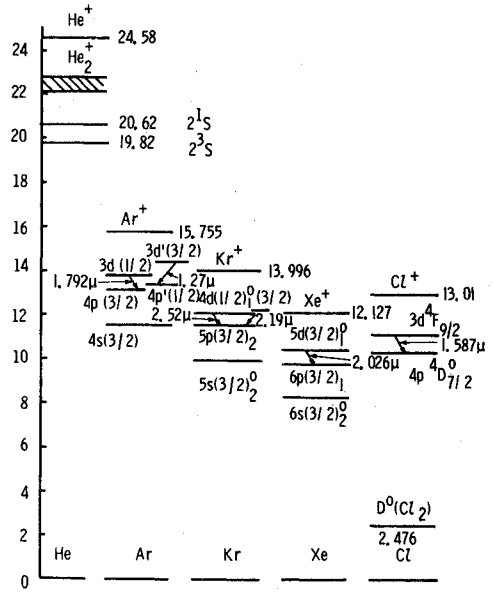

Fig. 17 Energy level diagram of nuclear volume-pumped lasers. Lasing species form a Penning mixture with He(2^3s) metastables. Charge transfer from He^+ (He_2^+) is a major mechanism for pumping the lasing species.

When the laser output was determined as a function of Ar or Xe concentration, it was found that both the nuclear-pumped and the electrically-pulsed afterglow lasers exhibited the same concentration dependence; therefore, the dominant atomic and molecular processes should be the same for both laser plasmas. This behavior is shown in Fig. 14 for He-Ar where nuclear-pumped and afterglow lasing (1.79 μm) are shown after normalization. If the TEA afterglow laser output at 400 Torr He-Ar is compared to the direct nuclear-pumped laser ouput at 400 Torr, there is a very close correlation. Likewise, Fig. 15 shows the direct nuclear-pumped ^{3}He-Xe (2.026 μm) laser output as a function of Xe concentration normalized with TEA afterglow lasing for varying total pressures. Note that at the higher pressures (>300 Torr) there is very good agreement between the afterglow and direct nuclear-pumped lasing results.

Using the electrically pulsed afterglow simulation future nuclear lasers can be predicted. All nuclear lasers discussed in this study were found to lase, at the specified wavelength, in the electrically pulsed high-pressure afterglow discharge. One laser, the He-F (~7000 Å FI) system, was found to lase only weakly in the afterglow, as shown in Fig. 16. Note the close coincidence between the current pulse and laser output which suggests that direct electron impact excitation of the upper laser level should be a dominant excitation mechanism. When this laser system was pulsed at the reactor, no lasing was observed for F concentrations from 0.001% to 1% and total pressures up to 1 atm. From laboratory TEA laser experiments this result was to be expected. Therefore, all lasers that exhibit lasing in the afterglow region at high pressures appear to be good candidates for direct nuclear pumping. Also, once a good candidate is chosen, the optimum concentration of lasing species can be determined from the electrically pulsed afterglow laser.

Excitation Mechanisms

From the energy level diagram of Fig. 17, it is noted that all the lasing gases form a Penning mixture with helium 2^1S and 2^3S metastables. One of the dominant laser excitation mechanism is, therefore, most probably Penning ionization of Ar, Xe, Kr, and Cl, by either atomic or molecular helium metastables. Atomic ions can also be created efficiently by charge transfer from He_2^+. As a result of these processes, large production rates of atomic ions occur followed by collisional radiative recombination, and then radiative cascade into the upper laser level. Collisional radiative recombination takes place very rapidly after the production of atomic ions since the electron temperature in a typical nuclear-induced plasma is near room temperature. This is shown in Fig. 18, which was

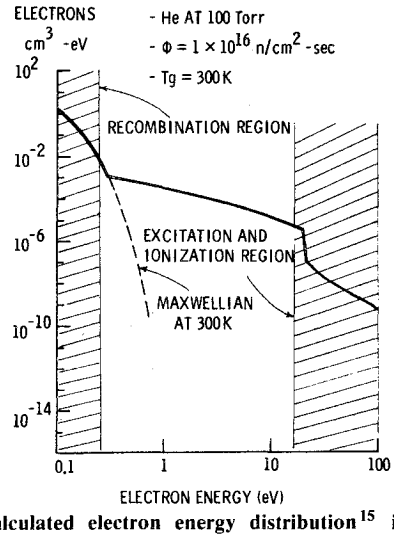

Fig. 18 Calculated electron energy distribution[15] indicating the regions of excitation-ionization and of recombination where most electrons reside. It is apparent that recombination can play a dominant role in populating upper laser levels.

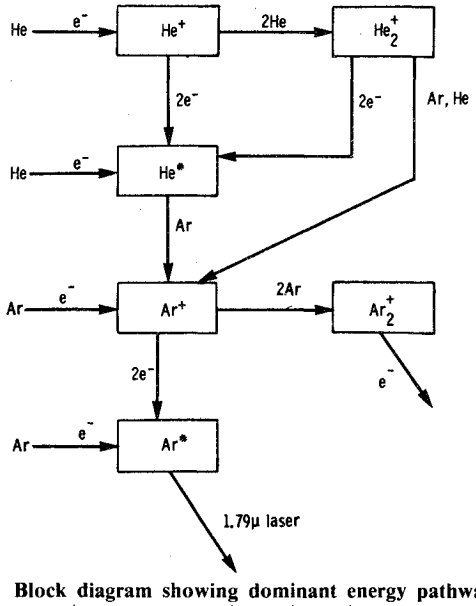

Fig. 19 Block diagram showing dominant energy pathways. High densities of Ar^+ (similarly, Xe^+, Kr^+, Cl^+) can be created from Penning ionization by He metastables and charge transfer from He_2^+. The Ar^+ is lost either by collisional-radiative recombination, thus feeding the upper laser level, or by Ar_2^+ formation which is a loss to lasing at 1.79 μm.

taken from the work of Hassan and Deese.[15] The electron energy distribution is characterized by two regions, an excitation-ionization region (electrons of high energy) and a recombination region (electrons near room temperature). The bulk of the electrons are in the recombination region and thus recombination becomes a very important pumping mechanism for direct nuclear-pumped lasers.[16]

Figure 19 shows a simplified energy flow diagram for the ^{3}He-Ar direct nuclear-pumped laser. Since the majority of the gas is helium, most of the energy deposited in the laser cell is deposited initially in helium (at least for the low concentrations of Ar). The secondary electrons created by the proton and tritium ions ionize helium, which then quickly forms He_2^+ ions from helium atomic ions.[17] At high pressures large densities of helium metastables can exist in the nuclear-pumped plasma.[18] These metastables collide with and Penning ionize neutral argon. Atomic argon ions are also efficiently produced by charge transfer with He_2^+. The Ar^+ species can then undergo one of two reactions, as shown in Fig. 19. It can recombine by collisional radiative recombination with the thermal electrons and then by radiative cascade populate the upper laser level. The lifetime of the upper laser level is longer than the lower laser level, thus, a population inversion is established. The Ar^+ ion can also form Ar_2^+ in a three-body collision, which is followed by dissociative recombination. The majority of the atomic states that are populated by dissociative recombination are lower than the upper laser level and, thus, the formation of Ar_2^+ is a loss mechanism for Ar^+ which in turn is a loss mechanism for lasing at 1.79 μm in Ar.

The Ar^+ steady-state density can be written as:

$$d[Ar^+]/dt = [He(m)][Ar]k_1 + [He_2^+][Ar][He]k_2 - [Ar^+][Ar][He]k_3 - [e^-]^2[Ar^+]k_4 - [Ar^+][Ar]^2k_5 = 0 \quad (1)$$

where the k's are rate coefficients for the following processes:

k_1: Penning ionization by He metastable (Ref. 19)

k_2: charge transfer from He_2^+ (Ref. 20)

k_3: Ar_2^+ formation, He stabilized (Ref. 21)

k_4: collisional radiative recombination of Ar^+ (Ref. 22)

k_5: Ar_2^+ formation, Ar stabilized (Ref. 23)

The He(2^{3}S) and electron densities were taken from the work of Guyot.[18] The Ar^+ density obtained from Eq. (1) has been plotted as a function of Ar concentration in Fig. 5 after normalization to the experimental data. There is good agreement between the calculated Ar^+ density and the experimental nuclear lasing results, thus the above-mentioned processes are probably the dominant pumping mechanisms.

The same argument presented for Ar can also be used to explain the ^{3}He-Xe nuclear laser results. Using the same equation as for Ar^+, but with Xe reaction rate coefficients, the calculated Xe^+ density was normalized to the experimental data in Fig. 10. There is not as good an agreement with experimental results as for the Ar system, nevertheless, the dominant excitation mechanisms appear to be the same.

Conclusions

Direct nuclear pumping of ^{3}He-Ar, Xe, Kr, and Cl has been demonstrated using the ^{3}He(n,p)^{3}H nuclear reaction for power deposition. High power homogeneous plasmas have been created at pressures up to 4 atm, which indicates that volumetric nuclear excitation is a convenient means of generating high pressure laser plasmas. Since nearly all laser systems operate with helium, it is convenient to replace the ^{4}He with ^{3}He and subject the gas to an intense neutron flux.

Peak laser output to date has been achieved in ^{3}He-Ar (1.79 μm) with 3.7 W while the lowest lasing flux threshold was achieved with the ^{3}He-Xe (2.026 μm) nuclear laser. Unfortunately, the ^{3}He-Kr system demonstrated a very high lasing flux threshold, probably due to competition effects between the 2.52 μm and 2.19 μm lasing transitions. The chlorine system lased at 1.587 μm at peak powers much lower than either the ^{3}He-Ar or ^{3}He-Xe systems.

It was found that all these laser systems lased in the high-pressure electrically-pulsed afterglow plasma. Although new laser systems which are unique to nuclear pumping may yet be found, the present systems lase readily in the electrically generated plasma. By studying the afterglow plasma, which has the same physical characteristics (except the time-dependent nature of the pulsed afterglow) as the nuclear generated plasma, the nuclear laser output could be optimized

with respect to lasing gas concentration. This technique is important because parameter studies at the reactor environment are very costly and time consuming, also new candidates for nuclear pumping can more readily be found and studied using the afterglow laser.

By using a simple kinetic model, it was found that the dominant pumping mechanisms are the creation of Ar^+, for instance, by charge transfer and Penning ionization followed by collisional-radiative recombination of Ar^+ and then radiative cascading into the upper laser level. When the concentration of lasing species becomes too high, formation of Ar_2^+ results and, as a consequence, laser output decreases. Although this simple model predicts collisional-radiative recombination as the dominant mechanism, in reality other processes may be dominant and future experimental results are required to substantiate the exact lasing mechanism.

Acknowledgment

We appreciate J. Fryer's diligence and craftsmanship and the support of the U.S. Army's Aberdeen Pulse Radiation Facility Staff which helped insure the success of this research.

References

[1] Thom, K. and Schneider, R. T., "Nuclear Pumped Gas Lasers," *AIAA Journal*, Vol. 10, April 1972, pp. 400-406.

[2] Lubkin, G. B., "Space Vehicles Could be Propelled by Remote Lasers," *Physics Today*, Vol. 30, Aug. 1977, pp. 17-20.

[3] McArthur, D. A. and Tollefsrud, P. B., "Observation of Laser Action in CO Gas Excited Only by Fission Fragments," *Applied Physics Letters*, Vol. 26, Feb. 15, 1975, pp. 187-190.

[4] Helmick, H. H., Fuller, J., and Schneider, R. T., "Direct Nuclear Pumping of a Helium-Xenon Laser," *Applied Physics Letters*, Vol. 26, March 15, 1975, pp. 327-328.

[5] DeYoung, R. J., Wells, W. E., Miley, G. H., and Verdeyen, J. T., "Direct Nuclear Pumping of a Ne-N_2 Laser," *Applied Physics Letters*, Vol. 28, May 1, 1975, pp. 519-521.

[6] Akerman, M. A., Miley, G. H., and McArthur, D. A., "A Helium-Mercury Direct Nuclear Pumped Laser," *Applied Physics Letters*, Vol. 30, April 15, 1977, pp. 409-412.

[7] DeYoung, R. J., Wells, W. E., and Miley, G. H., "Optioptical Gain in a Neutron-Induced ^{3}He-Ne-O_2 Plasma," *Applied Physics Letters*, Vol. 28, Feb. 15, 1976, pp. 194-197.

[8] DeYoung, R. J., Jalufka, N. W., Hohl, F., and Williams, M. D., "Direct Nuclear Pumped Lasers Using the Volumetric ^{3}He Reaction," *Proceedings of the Princeton University Conference on Partially Ionized Plasmas*, Sept. 1976, pp. 96-101.

[9] Jalufka, N. W., DeYoung, R. J., Hohl, F., and Williams, M. D., "Nuclear-Pumped ^{3}He-Ar Laser Excited by the ^{3}He(n,p)^{3}H Reaction," *Applied Physics Letters*, Vol. 29, Aug. 1, 1976, pp. 188-190.

[10] DeYoung, R. J., Jalufka, N. W., and Hohl, F., "Nuclear Pumped Lasing of ^{3}He-Xe and ^{3}He-Kr," *Applied Physics Letters*, Vol. 30, Jan. 1977, pp. 19-21.

[11] Mansfield, C. R., Bird, P. F., Davis, J. F., Wimett, R. F., and Helmick, H. H., "Direct Nuclear Pumping of a ^{3}He-Xe Laser," *Applied Physics Letters*, Vol. 30, June 15, 1977, pp. 640-641.

[12] Newman, L. A. and DeTemple, T. A., "High-Pressure Infrared Ar-Xe Laser System: Ionizer-Sustainer Mode of Excitation," *Applied Physics Letters*, Vol. 27, Dec. 15, 1975, pp. 678-680.

[13] Wood, O. R., Burkhardt, E. G., Pollack, M. A., and Birdges, T. J., "High-Pressure Laser Action in 13 Gases with Transverse Excitation," *Applied Physics Letters*, Vol. 18, March 15, 1971, pp. 261-264.

[14] English, J. R., Gardner, H. C., and Merritt, J. A., "Pulsed Stimulated Emission from N, C, Cl, and F Atoms," *IEEE Journal of Quantum Electronics*, Vol. QE-8, Nov. 1972, pp. 843-844.

[15] Hassan, H. A. and Deese, J. E., "Electron Distribution Function in a Plasma Generated by Fission Fragments," *The Physics of Fluids*, Vol. 19, Dec. 1976, pp. 2005-2011; see also: Lo, R. and Miley, G. H., "Electron Energy Distribution in a Helium Plasma Created by Nuclear Radiation," *IEEE Transactions on Plasma Science*, Vol. PS-2, Dec. 1974, pp. 198-205.

[16] Cooper, G. W. and Verdeyen, J. T., "Recombination-Pumped Atomic Nitrogen and Carbon Afterglow Lasers," *Journal of Applied Physics*, Vol. 48, March 1977, pp. 1170-1175.

[17] Deloche, R., Monchicourt, P., Cheret, M., and Lambert, F., "High-Pressure Helium Afterglow at Room Temperature," *Physical Review*, Vol A 13, March 1976, pp. 1140-1176.

[18] Guyot, J. C., Miley, G. H., and Verdeyen, J. T., "Metastable Densities in Noble-Gas Plasmas Created by Nuclear Radiation," *Journal of Applied Physics*, Vol. 42, Dec. 1971, pp. 5379-5391.

[19] Schmeltekopf, A. L., and Fehsenfled, F. C., "De-Excitation Rate Constants for Helium Metastable Atoms with Several Atoms and Molecules," *Journal of Chemical Physics*, Vol. 53, Oct. 15, 1970, pp. 3173-3177.

[20] Lee, F. W., Collins, C. B., and Waller, R. A., "Measurement of the Rate Coefficients for the Bimolecular and Thermolecular Charge Transfer Reactions of He_2^+ with Ne, Ar, N_2, CO, CO_2, and CH_4," *Journal of Chemical Physics*, Vol. 65, Sept. 1976, pp. 1605-1615.

[21] Bohme, D. K., Dunkin, D. B., Fehsenfeld, F. C. and Ferguson, E. E., "Flowing Afterglow Studies of Ion-Molecule Association Reactions," *Journal of Chemical Physics*, Vol. 51, Aug. 1969, pp. 863-872.

[22] Chen, C. J., "Collisional-Radiative Electron-Ion Recombination Rate in Rare-Gas Plasmas," *Journal of Chemical Physics*, Vol. 50, Feb. 1969, pp. 1560-1577; see also: Collins, C. G., "Collisional-Radiative Recombination of Ions and Electrons in High-Pressure Plasmas in which the Electron Temperature Exceeds the Gas Temperature," *Physical Review*, Vol. 177, Jan. 1969, pp. 254-257.

[23] Smith, D., Dean, A. G., and Plumb, E. C., "Three Body Conversion Reactions in Pure Rare Gases," *Journal of Physics B*, Vol. 5, Nov. 1972, pp. 2134-2142.